# TEMPO at Night

James L Carr[1], Heesung Chong[2], Xiong Liu[2], John C Houck[2], Virginia L. Kalb[3], Houria Madani[1], Dong L. Wu[4], Daniel Lindsey[5], Steven D. Miller[6], David E. Flittner[7], Kelly V. Chance[2], Raid Suleiman[2], John E Davis[2], Jean Fitzmaurice[2], and Laurel Carpenter[2]

[1]Carr Astronautics Corporation
[2]Harvard-Smithsonian Center for Astrophysics
[3]NASA Goddard Space Flight Center
[4]NASA/Goddard Space Flight Center
[5]NOAA/NESDIS/RAMMB
[6]Colorado State University
[7]NASA Langley Research Center

December 21, 2024

**Abstract**

The NASA Tropospheric Emissions: Monitoring of Pollution (TEMPO) instrument is hosted on a geostationary commercial communications satellite. TEMPO is an imaging spectrometer with primary mission to measure trace-gas concentrations from the observed spectra of reflected sunlight over the Continental United States and parts of Canada, Mexico, and the Caribbean. TEMPO produces an ultraviolet (UV, 293 nm - 494 nm) and a visible (538 nm - 741 nm) spectrum for each spatial pixel. TEMPO saw first light in August 2023. At night, TEMPO can observe city lights, gas flaring, maritime lights from fishing and offshore oil platforms, clouds and snow in the moonlight, lightning, aurorae, and nightglow without interfering with its primary daytime air quality/chemistry mission. This paper describes the capabilities of TEMPO to make nighttime observations and surveys of some early results. Repetitive coverage of North America enables production of clearest-sky composites that are similar to VIIRS Day-Night Band (DNB) "Black Marble" products. Spectra of urban areas contain spectral signatures of artificial lighting of various types that allow the radiance from each class of lighting to be estimated. Moonlight imaging of clouds provides a useful capability for discriminating clouds and fog. Lightning illuminating cloud tops from below is seen with distinct spectral features. Gas flares, associated with oil production, are observed and flare temperatures can be estimated from their spectra. Known auroral and nightglow spectral lines of atomic oxygen and molecular nitrogen are seen in the UV and visible spectra. The sodium d-layer is also observed.

# TEMPO at Night

**James L. Carr[1], Heesung Chong[2], Xiong Liu[2], John C. Houck[2], Virginia Kalb[3], Houria Madani[1], Dong L. Wu[3], Daniel T. Lindsey[4], Steven D. Miller[5], David E. Flittner[6], Kelly Chance[2], Raid Suleiman[2], John E. Davis[2], Jean Fitzmaurice[2], Laurel Carpenter[2]**

[1]Carr Astronautics, Greenbelt, MD, USA.

[2]Smithsonian Astrophysical Observatory (SAO), Center for Astrophysics | Harvard & Smithsonian, Cambridge, MA, USA.

[3]NASA Goddard Space Flight Center (GSFC), Greenbelt, MD, USA.

[4]National Oceanic and Atmospheric Administration/National Environmental Satellite, Data, and Information Service (NOAA/NESDIS), Fort Collins, CO, USA

[5]Cooperative Institute for Research in the Atmosphere (CIRA), Colorado State University, Fort Collins, CO, USA

[6]NASA Langley Research Center, Hampton, VA, USA

Corresponding author: J. L. Carr (jcarr@carrastro.com)

**Key Points:**

- TEMPO, intended to measure trace gases in daylight from geostationary orbit, has excellent capabilities for nighttime observations too.
- We show examples of city lights, nightglow and aurorae, moonlit clouds, gas flares, and lightning observations made by TEMPO.
- UV/Visible spectra enable classification of city lights, estimation of flare temperatures, and study of aurorae, nightglow and lightning.

## Abstract

The NASA Tropospheric Emissions: Monitoring of Pollution (TEMPO) instrument is hosted on a geostationary commercial communications satellite. TEMPO is an imaging spectrometer with primary mission to measure trace-gas concentrations from the observed spectra of reflected sunlight over the Continental United States and parts of Canada, Mexico, and the Caribbean. TEMPO produces an ultraviolet (UV, 293 nm – 494 nm) and a visible (538 nm – 741 nm) spectrum for each spatial pixel. TEMPO saw first light in August 2023. At night, TEMPO can observe city lights, gas flaring, maritime lights from fishing and offshore oil platforms, clouds and snow in the moonlight, lightning, aurorae, and nightglow without interfering with its primary daytime air quality/chemistry mission. This paper describes the capabilities of TEMPO to make nighttime observations and surveys of some early results. Repetitive coverage of North America enables production of clearest-sky composites that are similar to VIIRS Day-Night Band (DNB) "Black Marble" products. Spectra of urban areas contain spectral signatures of artificial lighting of various types that allow the radiance from each class of lighting to be estimated. Moonlight imaging of clouds provides a useful capability for discriminating clouds and fog. Lightning illuminating cloud tops from below is seen with distinct spectral features. Gas flares, associated with oil production, are observed and flare temperatures can be estimated from their spectra. Known auroral and nightglow spectral lines of atomic oxygen and molecular nitrogen are seen in the UV and visible spectra. The sodium d-layer is also observed.

## Plain Language Summary

NASA's TEMPO instrument operates over the equator at 91ºW longitude from a commercial communications satellite. During daytime, it measures the concentrations of trace gases and pollutants in the atmosphere. At night, it collects images of city lights, aurorae, moonlit clouds, gas flares, light from ships, and lightning. TEMPO makes a spectrum of the light from each pixel, and this enables a host of applications such as spectral classification of city lights to map usage of LED, high pressure sodium, and other types of artificial lighting, which has implications for health, ecology, and light pollution mitigation. Many spectral features can be seen in the spectra of aurorae, night glow, and lightning, and the temperature of gas flares can be measured.

## 1 Introduction

The Tropospheric Emissions: Monitoring of Pollution (TEMPO) instrument is the first NASA Earth Venture Instrument (EVI) in the EVI program. Its primary mission relates to air quality with measurements of the major elements (or their proxies) in the tropospheric ozone cycle, column concentrations of trace gases such as $NO_2$, $O_3$, and HCHO by the spectral fingerprints these gases leave in reflected sunlight, and observations of aerosols such as smoke and dust (Zoogman et. al., 2017). TEMPO is positioned at 91ºW longitude in a geostationary orbit where it is hosted on the commercial communication satellite Intelsat-40e. TEMPO saw first light in August 2023. TEMPO Level -1, -2, and -3 products are continuously produced at the Smithsonian Astrophysical Observatory (SAO) in Cambridge MA. The latest Version 3 products have achieved provisional maturity and are archived at the NASA Atmospheric Science Data Center (ASDC) where they are publicly accessible.

The same radiometric sensitivity that enables TEMPO to retrieve small trace gas concentrations from subtle changes in the spectra of reflected sunlight also makes TEMPO capable of low light observing at night. Early calculations (Carr et. al., 2017) demonstrated TEMPO's sensitivity, in principle, to discriminate between various lighting types based on their spectral signatures. Low light observing can be pursued without interfering with the main mission of TEMPO, which is performed entirely in daylight, and became the subject of a "green paper" describing additional investigations possible with TEMPO (Chance et. al., 2019). TEMPO was never designed for nighttime operations and there were significant challenges that had to be overcome to gather high-quality science data. These include dark background subtraction, detector noise, straylight from the bright side of the terminator, and geolocation of nighttime data. This paper describes TEMPO's low light observing capabilities and showcases several application areas where TEMPO can make significant contributions.

Satellite remote sensing of the Earth at night offers a unique perspective, revealing both anthropogenic and natural light phenomena that cannot be observed in the daytime (Levin et. al., 2020). The Visible Infrared Imaging Radiometer Suite (VIIRS) instruments onboard the joint NASA/NOAA Suomi National Polar-orbiting Partnership (Suomi NPP), NOAA-20, and NOAA-21 satellites have a Day/Night Band (DNB) that is capable of low light detection at night (VIIRS-DNB). NASA's Black Marble products (BlackMarble) provide global gridded daily measurements from the DNB that are suitable for Earth system science and applications studies. For example, Black Marble products are used for estimating population (Martinez et. al., 2023), tracking power outages and recovery (Wang et. al., 2018), monitoring disasters (Zhang et. al. 2023) and conflict (Yu et. al., 2023), understanding biological impacts of increased light pollution (Ditmer et. al., 2021) and identifying gas flaring activities (Chakraborty et. al., 2023). These observations expand many current applications and enable new ones (Miller et. al., 2013).

VIIRS-DNB collects data in the visible to near-infrared part of the spectrum (400-900 nm), which is suitable for the afore-mentioned nighttime lights applications, but as a broadband sensor, it cannot identify the lighting source. The TEMPO nighttime lights observations capture the full spectral information from nominally 290-490 nm and 540-740 nm, albeit at a coarser spatial resolution. The synergy between the two instruments is compelling, potentially enabling attribution of lighting type (e.g., artificial light vs gas flaring, Light Emitting Diode (LED) versus high pressure sodium lamps) for use with Black Marble applications.

## 2 Materials and Methods

### 2.1 TEMPO Instrument

TEMPO is an imaging spectrometer that covers the Continental United States and parts of Canada, Mexico, and the Caribbean. Its spectrometer produces an ultraviolet (293 nm – 494 nm) and a visible (538 nm – 741 nm) spectrum for each spatial pixel sampled every ~0.2 nm and with a Full Width Half Maximum (FWHM) spectral resolution of approximately ~0.6 nm. TEMPO spatial footprints are approximately 4.75 km (East-West) by 2 km (North-South) at the center of its field of regard. TEMPO executes a step-scan from East to West and generally repeats its continental coverage once per hour in daylight. Its scan mirror is stabilized using gyroscopes that sense spacecraft motion during the exposure at each step. Light reflected off the scan mirror enters a telescope and then the spectrometer through a slit, is dispersed by a grating, and falls on side-by-side two-dimensional Charged Coupled Devices (CCDs), one for the visible (VIS) wavelengths and the other for the ultraviolet (UV). The two CCD frames captured at each step measure 2048 spatial pixels North to South, each with 1028 spectral samples. TEMPO performs an irradiance calibration by viewing the sun through a transmissive diffuser and collects dark frames with its aperture closed nightly.

### 2.2 Scheduling Nighttime Observations

Nighttime observations with TEMPO can be scheduled when there is no conflict with the primary atmospheric chemistry mission, and when instrument safety constraints are satisfied. The primary mission requires scanning sunlit areas whenever any part of the field of regard has solar zenith angle below 70 degrees. An important instrument safety constraint requires that the aperture remain closed while the sun is within 60 degrees of the instrument boresight vector. Within these constraints, the longest windows of opportunity for nighttime observations occur near the winter solstice. Conversely, opportunities for nighttime observations are severely limited or ruled out during a two-month period, May 20-July 20, centered on the summer solstice. When the observation window is narrow, nighttime scans must be short and are likely contaminated by scattered sunlight in the field of regard. With this in mind, we plan our nighttime observing between mid-August and mid-April.

Nighttime observations are scheduled during the early morning and late evening at the TEMPO spacecraft longitude. Morning scans see nighttime in the western end of the field of regard, while evening scans see nighttime in the eastern end.

On a given day, the start and end times for nighttime scans are set by the solar boresight angle safety constraint, and the interval devoted to radiance scanning of sunlit areas of the field of regard. In the morning, the safety constraint sets the earliest time when nighttime scans can start, and the start time of the first radiance scan defines the latest time at which nighttime scans can end. Within this window, the planning software schedules a whole number of scans between specified endpoints in the field of regard. Evening scans are scheduled in a similar way, to complete a whole number of nighttime scans before the safety constraint mandates that the aperture be closed.

If a desired region cannot be scanned within a single twilight opportunity, the region can be divided into sections that are scanned separately over several days. If the window of opportunity is too short to complete one scan, then no nighttime scan is scheduled.

### 2.3 Level 0 to Level 1 Processing

The raw TEMPO measurement data, downlinked from the satellite, are reconstructed and formatted on the ground to Level 0 data. The Level 0 files provide measurements in the digital count format. The TEMPO Level 0-1 processor converts the digital counts to physical quantities and stores them in Level 1 files. Nighttime Earth measurements are included in “twilight” radiance (RADT) Level 1 files.

During Level 0-1 processing, the digital counts are first converted to electric currents in units of electrons/s through multiple correction steps. The process starts with co-adding correction, where the digital counts are divided by the number of images co-added onboard. The number of co-adds for RADT measurements varies depending on uplink commands. The co-adding correction is followed by corrections for parameters related to the analog-to-digital converters, including electronic offset, non-linearity, electronic crosstalk, and gain, resulting in signals expressed in units of the number of electrons. Then, the L0-1 processor corrects for smear signals and divides the outputs by integration time, converting the units to electrons/s. Lastly, the photo response non-uniformity is corrected.

The following RADT processing step is the dark current correction. The precise estimation of dark current is especially important for RADT processing due to the low signal levels of nighttime radiances. Upon uplink commands, RADT scans are performed following dark current measurements, with consistent integration time and co-add settings to facilitate near-real-time dark subtraction. However, the dark currents vary with the temperature of the focal plane array (FPA), even within a short time frame, hindering the simple subtraction of pre-measured dark images from radiance images. Therefore, we scale the pre-measured dark current for each mirror step of the radiance measurements before subtraction to account for the FPA temperature variation. For scaling, we use the storage-region dark current as a parameter, assuming that the dark currents from both the photoactive and storage regions of the CCDs react consistently to the FPA temperature. Specifically, we calculate the ratio between the storage-region dark currents measured during the dark and Earth radiance exposures. This ratio serves as a scaling factor for the pre-measured photoactive-region dark current. The dark current scaling is conducted on a per-CCD-quadrant basis (VIS North, UV North, VIS South, and UV South).

After the dark current correction, the derived electric currents are multiplied by the pre-launch radiometric calibration coefficients. At this step, the unit of nighttime radiances is converted from electrons/s to Ph/(s $cm^2$ nm sr).

## 2.4 Level 1 Post Processing

Working with the low signal levels at night is very challenging. Nominal band integrated radiances in daylight are $2.4 \times 10^{15}$ and $2.5 \times 10^{15}$ Ph/(s $cm^2$ nm sr) for the VIS and UV bands respectively. City lights radiances are four to five orders of magnitude smaller and reflected moonlight is even smaller. Post processing is necessary to retrieve useful information even after careful Level 0-1 processing. Post processing mitigates the impact of noise bursts and subtracts unwanted background. The VIS and UV frames contain full spectra for each spatial pixel in their respective spectral ranges. A granule collects a variable number of VIS/UV frame pairs at each mirror step (typically on the order of 100 steps). The post processing described below has been implemented in Python available on GitHub.

Figure 1 illustrates the first post-processing cleanup steps starting from a Level-1 (L1) frame. We assign a post-processing Quality Flag (QF) to each CCD pixel of each frame using statistical anomaly tests taking into consideration that nighttime frames are generally expected to be dark. A QF value of zero indicates nominal data. The first step is identifying the persistently hot CCD pixels (QF=1). The spectral samples for each spatial pixel (a horizontal line across a frame in Figures 1a and 1d) are analyzed to find those that are 10σ over nominal. We count the number of times that happens for each CCD pixel across the granule. If it is more than three times, that CCD pixel is marked as persistently hot across all frames in the granule. We use the Median Absolute Difference (MAD) method to robustly estimate the mean value as the median and the effective sigma as 1.4826 times the median of the absolute value of differences with respect to the nominal value. This is a robust estimate of the sigma of a normally distributed main population (Huber and Ronchetti, 2011). The persistently hot pixels are generally found at the locations of known focal plane defects.

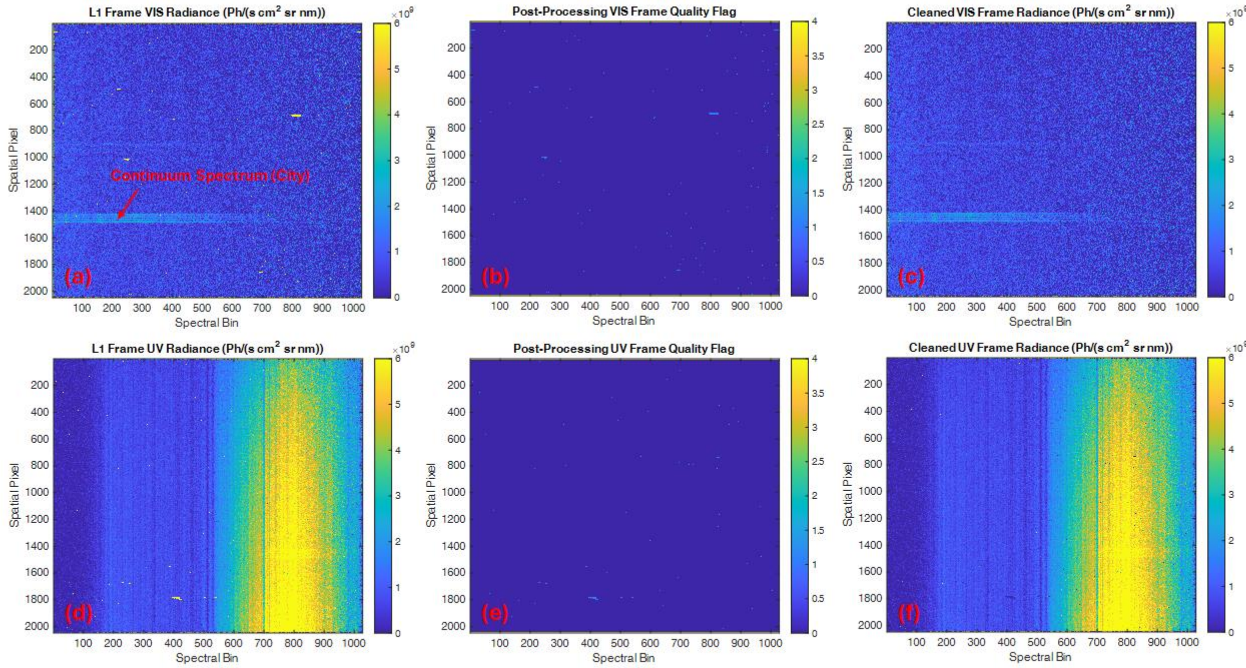


**Figure 1.** Frame cleanup starts with a VIS (a) or UV (d) frame from an L1 granule. Quality flags are assigned, (b) and (e), by a series of statistical anomaly tests. The cleaned frames (c) and (f) have the non-nominal quality CCD pixels masked. A large background remains, particularly in the UV band (f). Data shown is mirror step 92 from TEMPO_RADT_L1_V03_20240209T005321Z_S014G03.nc.

Anomalously noisy pixels (QF=2) are manifested as noise bursts in an otherwise dark CCD frame persisting for one or at most a few consecutive frames. Otherwise, the noise in a large majority of dark pixels is well understood in terms read noise and Poisson noise from the dark current. Identification of anomalously noisy data follows the identification of the persistently hot pixels. The spectral samples for each spatial pixel are analyzed in the same manner as previously, neglecting the persistently hot CCD pixels. A 6σ threshold is used to identify the anomalously noisy pixels. City lights are apparent as horizontal streaks across the frame, indicating a continuum spectrum concentrated at a spatial location. The robust estimate for sigma will be generally larger in these spatial pixels, so valid city lights data will not be marked as anomalous. Anomalously noisy pixels comprise a small minority of all pixels, likely related to the phenomenon of Random Telegraph Signal (RTS) error induced by radiation (Smith et. al., 2004).

The next QF test identifies over subtraction of dark current (QF=3). As explained in Section 2.3, we scale the estimated dark current, which is highly sensitive to detector temperature, based on the dark current observed in the storage region of the CCD. Radiation can affect the storage region as well as the active region. When this happens, the scaled dark charge to subtract from the active pixels is anomalously large and an entire focal plane quadrant is impacted. This is an infrequent event that is easily detected from the time series of median values of pixels in each quadrant across the granule using a 6σ MAD test. The last QF step is to mark edge pixels not recommended for use (QF=4).

When all pixels with QF > 0 are masked, a clean frame is produced as shown in Figures 1c and 1f. However, a significant residual background remains, particularly in the UV band. The background is modeled as the spatially smooth part of each spectral column for each column individually. The background model is a polynomial, generally of degree three, plus a step change at the midline dividing the top and bottom halves of the frame. The step corrects for possible residuals from the per-CCD-quadrant dark current correction (see Section 2.3). The polynomial-plus-step background model is fit using only QF = 0 pixels and excluding bright spatial pixels with city spectra (found with a 3σ MAD test) and the signal is what remains after background subtraction. The separation of signal from background is shown in Figures 2a-2d, emphasizing that effective background subtraction is essential for identifying city lights, especially in the UV band. Even though the signal is often smaller than the background, light from urban areas is easily identified, as illustrated in Figure 3.

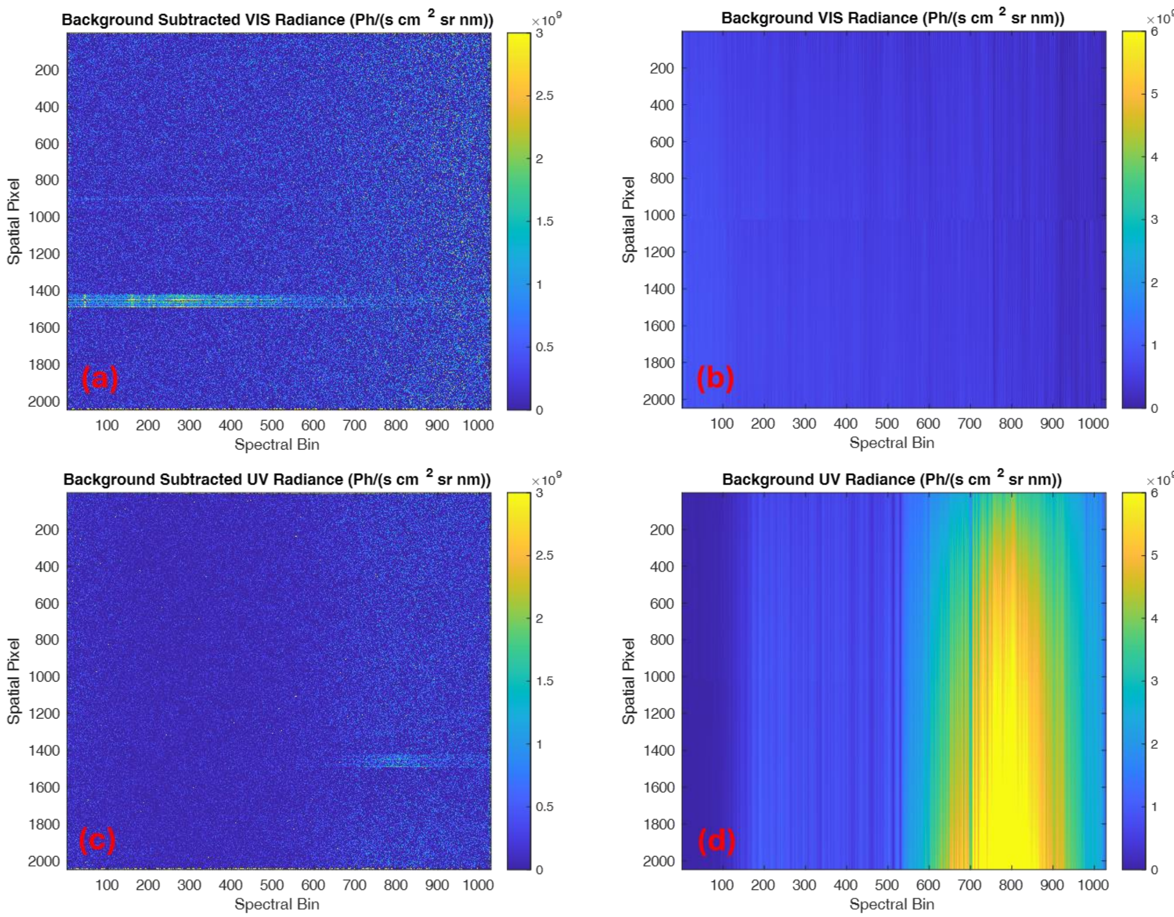


**Figure 2.** Separation of signal, (a) and (c), from background, (b) and (d). Data shown is mirror step 92 from TEMPO_RADT_L1_V03_20240209T005321Z_S014G03.nc. A cubic polynomial plus a step represents the background for each spectral column.

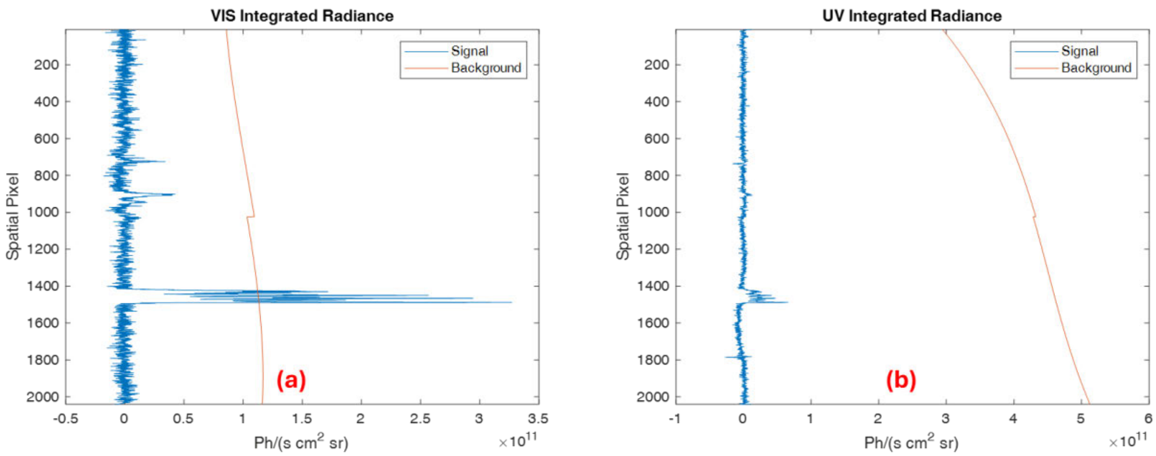


Radiance integrated across all wavelengths for step 92 of TEMPO_RADT_L1_V03_20240209T005321Z_S014G03.nc.

The background is a combination of light scattered into the optical path originating from the bright side of the terminator and residual dark charge. The former is evident from the spectra of background light as will be seen later in spatially averaged background spectra. The latter is evident from the same sinusoidal variations seen with the storage region dark current scaling driven by the heater cycling while controlling the focal plane temperature. The nature of the background will be explored further in Section 4.

## 3 Data

TEMPO nighttime data are available from ASDC. The Earth disk is always partially illuminated when collecting nighttime data since the TEMPO aperture must remain shut when the sun would be directly in front of TEMPO and the disk is completely dark, hence these radiances are designated as "twilight" radiances. There are two observing windows each night. The East Coast of the United States is covered after regular daytime observations complete on the West Coast and the West Coast of the United States is covered before daytime observations begin on the East Coast. A few nighttime observations were attempted in September and early October 2023 during TEMPO's commissioning, but regular collection of nighttime observations really started at the Winter Solstice and continued with a few gaps until the end of the first season in April 2024. Collections were made with exposures between 3 and 120 seconds. The longest exposures targeted auroral light with the scan mirror offset to point poleward. As the season comes to a close there is less available time for safe observing, so exposure times are reduced to allow for more coverage.

## 4 Results

Here we survey some early results from Season 1 to demonstrate the potential of TEMPO for nighttime observing, showing examples of monthly clearest-sky mosaics, spectral classification of artificial lights, moonlight imaging, aurorae, gas flares, and lightning.

### 4.1 City Lights

Before TEMPO first light, we gathered spectra of ambient light pollution reflected from clouds on overcast moonless nights to start developing tools for spectral classification. A cloud deck acts as a diffuse reflector to scatter light back to ground-based instruments. We employed a research-grade Pandora spectrometer instrument to conduct these observations. Most of the components of this Pandora are similar or identical to the standard instrument in the Pandora Global Network (PGN). Our spectrometer has an extended spectral range (300 nm to 1200 nm), slightly lower spectral resolution (1-2 nm) and was calibrated spectrally with known atmospheric and solar lines. Radiometrically, our instrument was calibrated against a NIST-traceable integrating sphere source at Goddard Space Flight Center (GSFC). Because of the weak signal, we averaged nighttime measurements for 5.1 minutes to improve the Signal to Noise Ratio (SNR).

Figure 4 is an observed zenith spectrum from GSFC on the moonless overcast night of April 1, 2024. Between 400 and 700 nm, Light Emitting Diode (LED) sources dominate the emission spectrum near the GSFC building. In addition, spectral features from Hg and Na are evident. These spectral features are quite repeatable on other cloudy nights, while their intensity may vary.

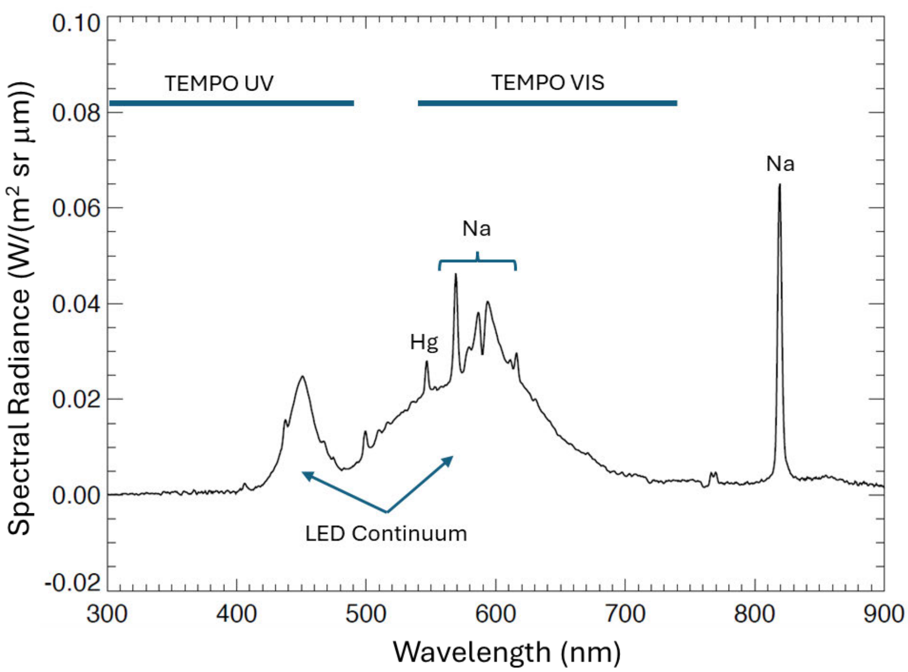


**Figure 4.** A spectrum from a zenith-viewing Pandora instrument on the roof of Building 33 at GSFC on 1 April 2024 19:19 local time under cloud cover with the moon set. The spectrum becomes increasingly noisy at wavelengths > 900 nm (not shown).

The Pandora spectra show larger signals in the range 540 nm to 640 nm covered by the TEMPO VIS band. We integrate our city lights spectra over this range to form our city lights imagery to avoid integrating noise where there is less signal. Figure 5 shows a full scan on a moonless night over a canvas of the nominal field of regard for nighttime scans. Land areas that are dark or blurry in appearance are cloud covered. We have converted radiances from photon to energy units to be compatible with the units commonly used when working with the VIIRS-DNB.


**Figure 5.** Single scan on a moonless night (9 February 2024 00:02Z) with spectral radiance converted from photon to energy units and integrated over the range 540 nm to 640 nm.

The geolocation tags applied during Level 0-1 processing at night are only nominal values and may deviate from ideal by several pixels. The regular Image Navigation and Registration (INR) for TEMPO was only designed to work during daytime and is more accurate. For more accurate geolocation at night, we measure our misalignment against a VIIRS-DNB monthly clear-sky mosaic to take advantage of the accurate geolocation of VIIRS (Lin et. al., 2022) and resample both to a standard TEMPO fixed grid. This has the added benefit of enabling fusion of TEMPO and VIIRS data for studies. A clearest-sky composite is shown in Figure 6. Here, scans from moonless nights have been registered to VIIRS-DNB and composited to take the brightest pixel from all scans at each site to have a good chance of selecting a cloud-free pixel from one of them. We use nearest neighbor resampling when registering TEMPO to VIIRS and keep track of the selected TEMPO pixel and granule from which it came so as to be able to access the spectrum for each pixel in the composite.

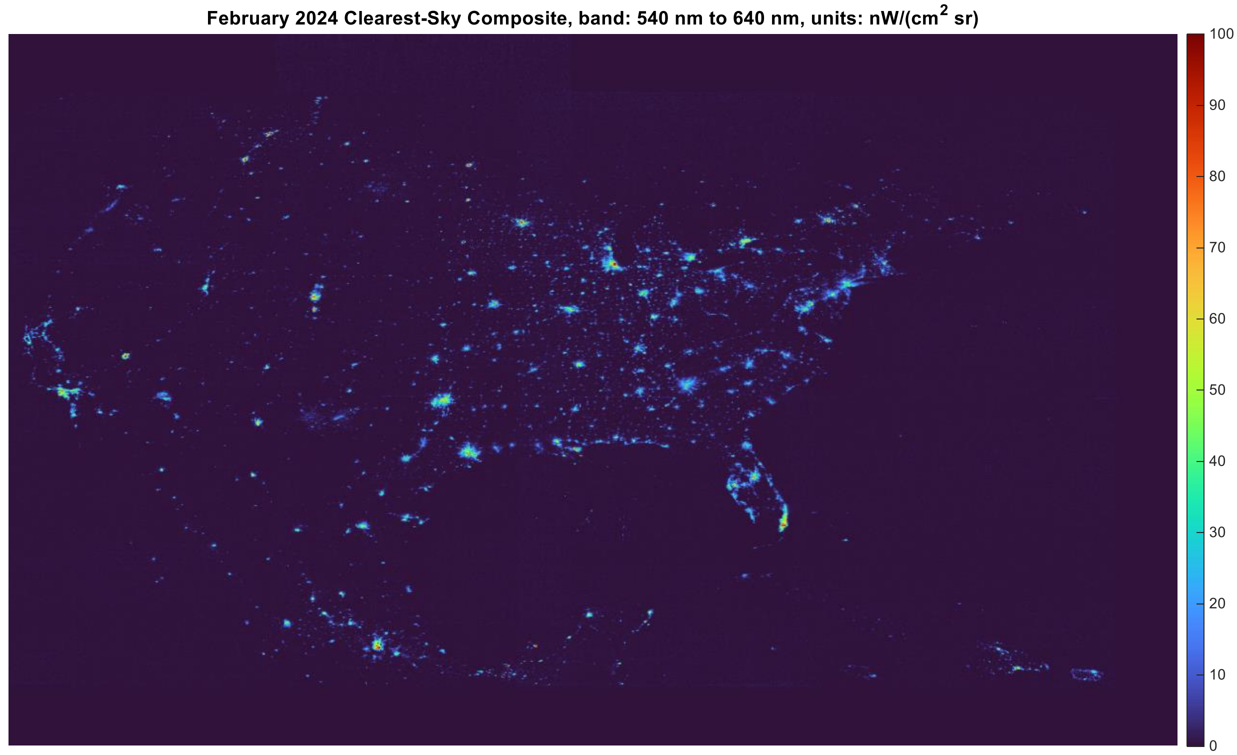


**Figure 6**. TEMPO composite for February 2024 moonless nights in the VIS band.

Figure 7 is the TEMPO UV clearest-sky mosaic for the same period. Using the TEMPO UV band is more challenging than the VIS band because of its larger background. We can gain insight into the nature of the VIS and UV backgrounds from their spectra, shown in Figure 8. The background has been separated from the city lights signal by the background subtraction post-processing step on a moonless night. We hypothesize that the background has a significant contribution from light from the bright side of the terminator that has been scattered into the optical path. The blue peak is emphasized due to Rayleigh scattering and there is good evidence of the solar Fraunhofer lines, including $O_2$ B and C, and Water Vapor (WV) absorption from the atmosphere.

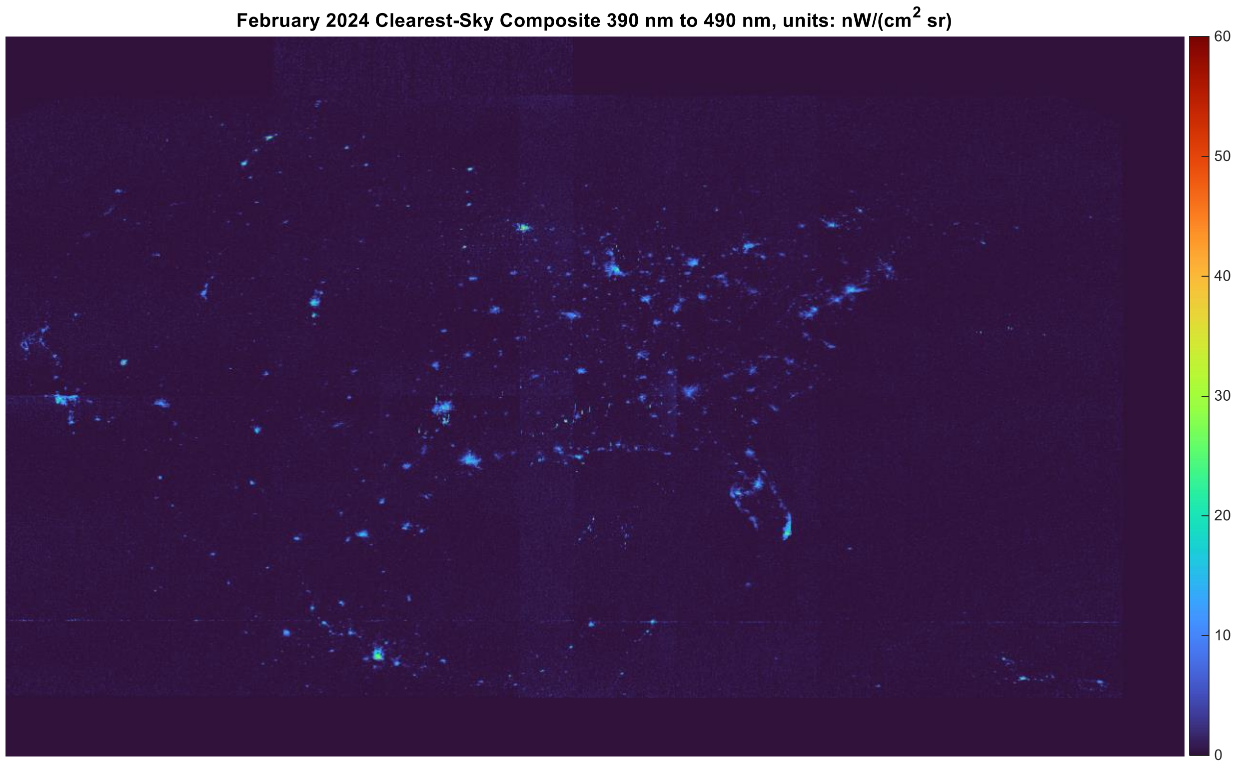


**Figure 7**. TEMPO composite for February 2024 moonless nights in the UV band.

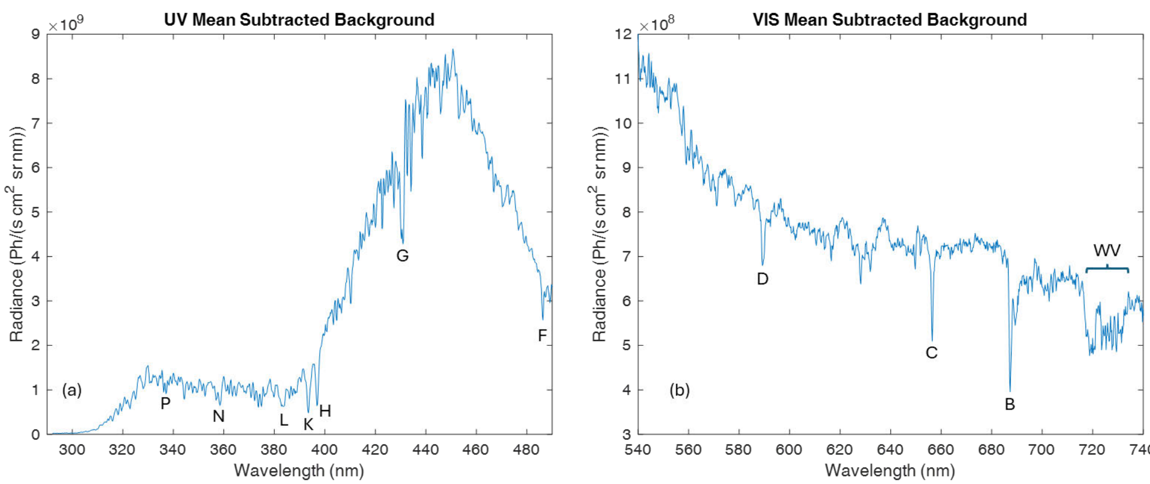


**Figure 8.** Background light in the UV (a) and VIS (b) bands averaged over a granule (9 February 2024 00:02Z) that have been annotated to show the Fraunhofer lines and atmospheric WV absorption.

Scans on moonless nights offer the opportunity to evaluate the radiometric noise in the band integrated TEMPO radiances from statistics over dark targets. Table 1 shows the mean (μ) and standard deviation (σ) for three exposure times over dark ocean. The spectral radiance has been integrated over a 100 nm range for each band (VIS: 540 nm – 640 nm; UV: 390 nm – 490 nm). The means are essentially zero, which indicates that the background has been effectively subtracted. Background subtraction will be slightly less effective when the moon is risen as some of the reflected moonlight risks being subtracted as background. Moonlight imaging is discussed in Section 4.2. The sigmas represent the sensitivities of the band integrated radiance to discern city lights.

**Table 1.** Statistics over dark targets without moonlight.

| | 2024-02-09 00:02 | | 2024-03-14 10:33 | | 2024-04-08 01:13 | |
|---|---|---|---|---|---|---|
| Exposure (s) | 12.6 | | 6.3 | | 3.0 | |
| Co-Adds | 2 | | 1 | | 1 | |
| Moon Illumination | 2%, Set | | 22%, Set | | 1%, Set | |
| Dark Target Statistics | μ | σ | μ | σ | μ | σ |
| VIS (nW/(cm$^2$ sr)) | 0.01 | 0.79 | 0.05 | 1.18 | 0.05 | 1.84 |
| UV (nW/(cm$^2$ sr)) | 0.02 | 1.03 | 0.02 | 1.37 | -0.01 | 2.54 |
| Noise Model NEDN | μ | σ | μ | σ | μ | σ |
| VIS (nW/(cm$^2$ sr)) | - | 0.78 | - | 1.10 | - | 1.78 |
| UV (nW/(cm$^2$ sr)) | - | 0.93 | - | 1.32 | - | 2.15 |

The dark-target noise statistics can be understood theoretically. The main noise contributors are CCD read noise, quantization, and Poisson noise from the dark current and background light. The dark current ($j_{dark}$) can be known from the dark collections taken prior to nighttime observing with the aperture closed and used for background subtraction in the L0-to-1 processing. The quantization error ($\sigma_q = 4.8$ e$^-$) and read noise ($\sigma_r = 49.7$ e$^-$) have been measured in the factory. Equation (1) is the model for the Noise-Equivalent Delta Radiance (*NEDN*) in a band-integrated radiance.

$$NEDN^2 = \left(1 + \frac{1}{N}\right) \sum_\lambda \left(\frac{j_{dark} \cdot T + n \cdot (\sigma_r^2 + \sigma_q^2)}{T^2} \cdot C^2 \cdot d\lambda^2\right) \quad (1)$$

The summation is over the spectral bins in the band, each with width $d\lambda = 0.2$ nm, $C$ is the radiometric calibration coefficient to convert photocurrent to spectral radiance, and $N$ is the number of frames in the dark collect averaged to measure the dark background (typically ~50). Equation (1) does not include the Poisson noise from the subtracted background, which depends on the distance to the bright side of the terminator and therefore will slightly underestimate the *NEDN*. Table 1 includes a modeled value for *NEDN* in the three cases. The dark current varies across the focal plane, so the median *NEDN* is reported. To optimize nighttime observations, it is best to use the longest possible integration time per co-add with the fewest co-adds ($n$) to make up the exposure ($T$). This minimizes the number of read-noise contributions going into the total exposure, but hardware limits the integration time to a maximum of 6.3 s, meaning that longer exposures must be constructed with multiple co-adds.

The most interesting feature of TEMPO at night is the ability to collect spectra for each spatial pixel, which allows classification of the content of light from urban areas, such as was done by the hyperspectral DLR Earth Sensing Imaging Spectrometer (DESIS) from the International Space Station (ISS) (Ryan et. al., 2024). Stepwise regression is used to fit the observed spectra with linear combinations of members of a spectral library. The algorithm tries adding a new spectrum from the library at each step, fits with the provisionally enlarged set of contributing members, and selects the provisional contributor that reduces the mean squared residuals the most but leaves all contributions positive. The positivity condition forces compliance with physical reality where there is no such thing as negative light (i.e., a light sink). The stepwise regression stops when it is no longer possible to enlarge the contributing set and improve the fit. The spectral range 540 nm to 640 nm of the VIS band is used to avoid longer wavelength atmospheric absorption features and the background subtraction challenges of the UV band.

The spectral library was assembled from a NOAA library lamp spectra (Elvidge, et. al., 2010) and a larger European library (Tapia, et. al., 2017). It has been organized according to a family-genus-species taxonomy. The families collect LED, fluorescent, halide, sodium, moonlit surfaces, and thermal (blackbody) sources. The genus groups individual species (i.e., individual lamps) within the family in accordance with their spectral signatures, which can be quite varied in the case of LEDs.

Figure 9 shows an example from Miami, Florida where the most prominent families found in the VIS spectrum of a bright pixel are LED, high-pressure sodium, halide, and fluorescent lighting. These families are the most frequently retrieved, in general, as can be seen in the classifications of the clearest-sky pixels for the moonless nights in February 2024 (Figure 10). LED lighting is the dominant family. Evidence of Hg (546.074 nm) and Na (568.635 nm) lines is present in many spectra. The spectral resolution of TEMPO (FWHM = ~0.6 nm) is finer than the spectral resolutions of the library spectra (3 nm for the NOAA spectra and 1.7 nm for the European spectra). Consequently, line-like spectral features will appear sharper in the TEMPO data and their observed peaks will not be exactly fit.

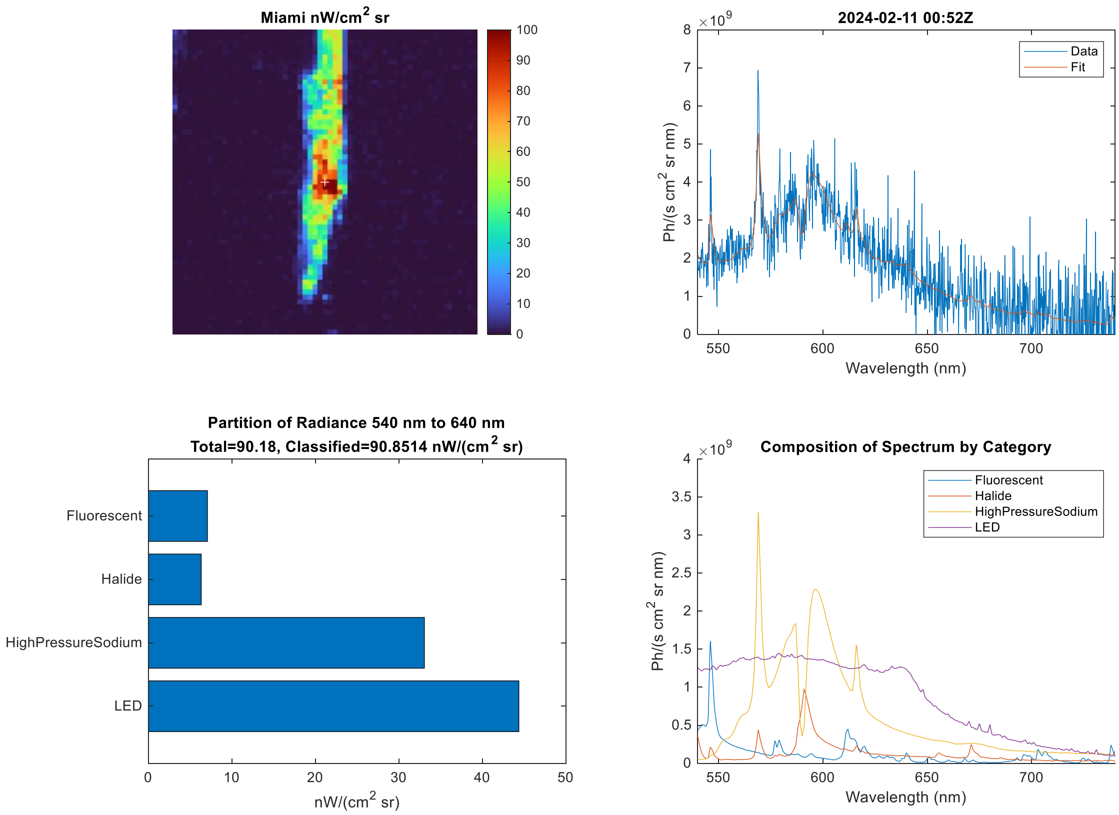


**Figure 9.** Spectral classification of the lights found a bright pixel near Miami, FL (TEMPO_RADT_L1_V03_20240211T005247Z_S012G03.nc, Step 94, Pixel 1691).

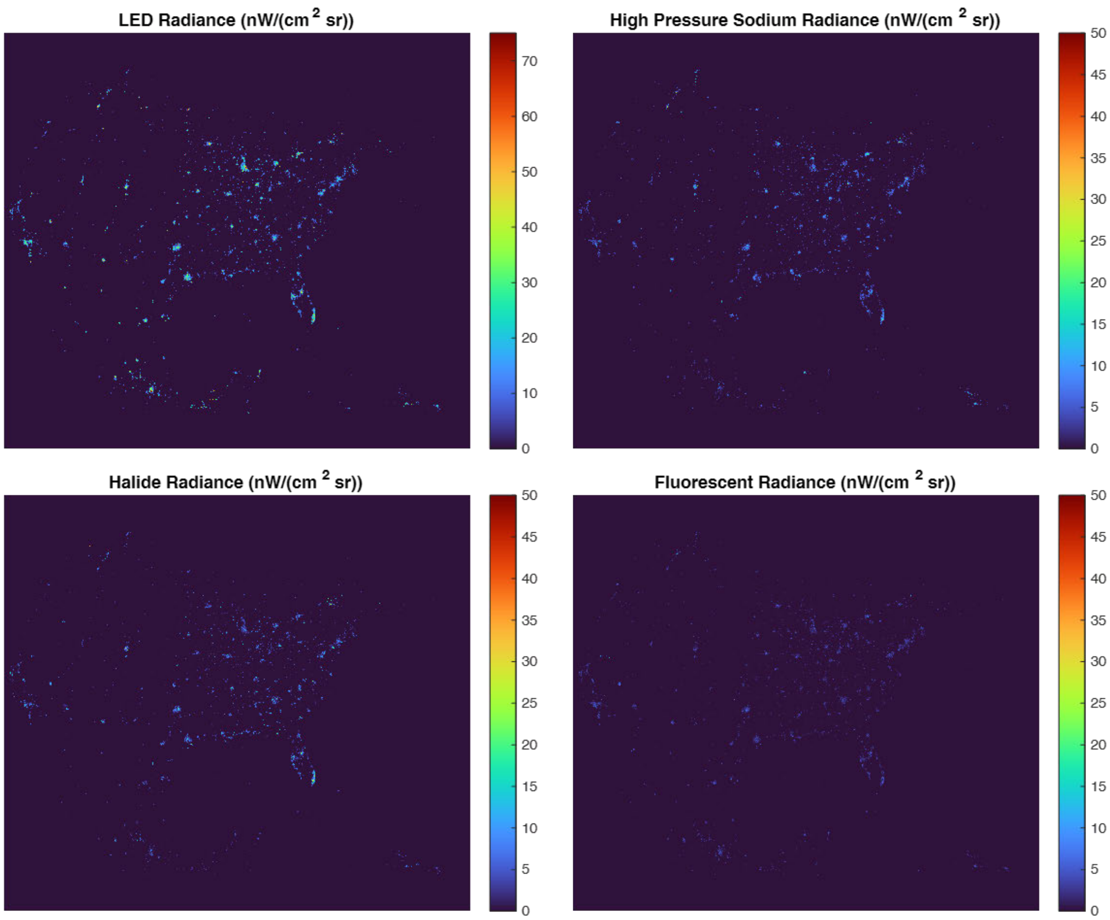


**Figure 10.** Radiance from each family of artificial lights seen across North America and the Caribbean. The radiance in each family is the sum of the radiance from the contributing members of that family.

## 4.2 Moonlight Imaging

Visible imaging under moonlight can be particularly useful for discerning clouds and fog, since infrared imaging can be challenged when low clouds and fog are nearly the same temperature as the underlying ground/water. The VIIRS-DNB has proven to be a useful tool for this purpose and for following nighttime smoke (Rogers et. al., 2023). Nighttime aerosol retrievals are also possible (Zhou et. al., 2021). These are potentially use cases for a future operational nighttime visible sensor in geostationary orbit. Figure 11 shows imagery from four scans under various illumination conditions. Because the lunar irradiance extends across the entire VIS band, we have integrated the radiance over the full range 540 nm to 740 nm, which is still less than the VIIRS-DNB passband. Clouds and illuminated land surfaces are observed at the low end of the radiance scale. The occasional vertical black bars are due to telemetry synchronization problems that have been resolved and are not expected to reoccur in data collected in our second season.

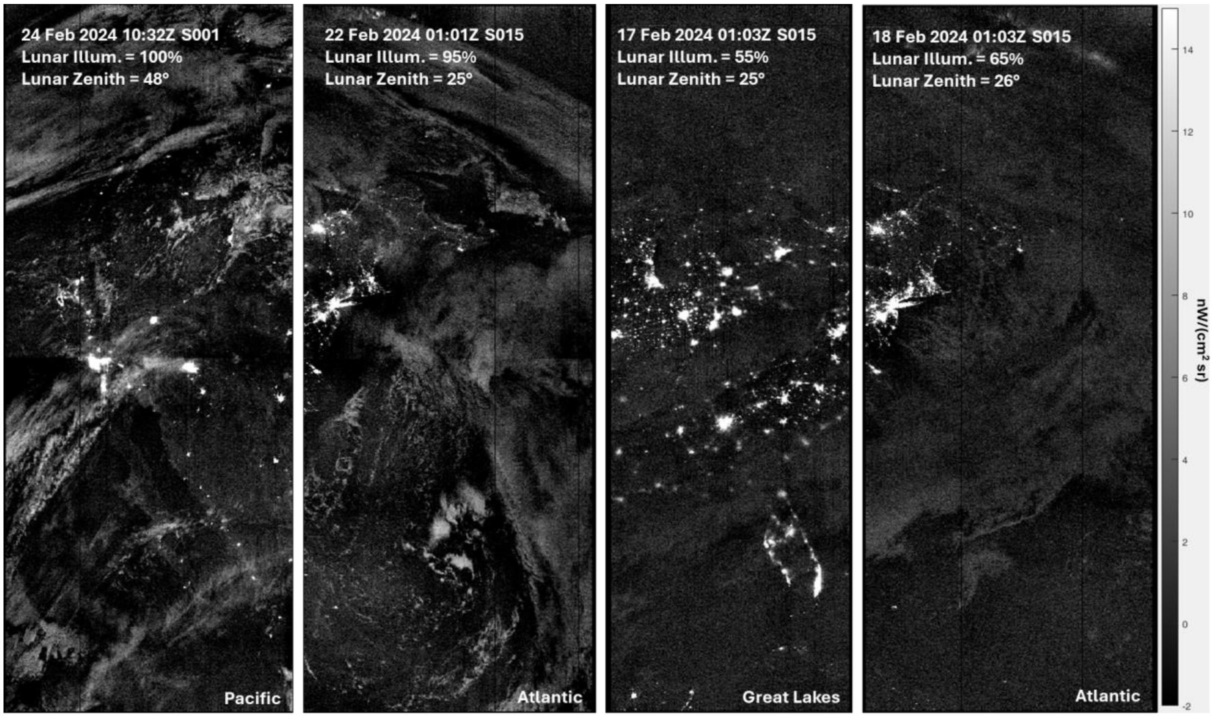


**Figure 11**. Scans under moonlight with the percentage of the moon illuminated and the lunar zenith angle at the midpoint of the last scan granule in the legends. Bright city lights are saturated with the grayscale maximum = 15 nW/(cm$^2$ sr) and land surfaces can be seen.

4.3 Nightglow and Auroral Light

TEMPO can tilt its field of regard northward to include pixels north of Hudson Bay as well as the Earth limb on the eastern and westernmost ends of the field of regard. The limb-viewing geometry in Figure 12 is very interesting as it offers a vertical profile. Only pixels above the surface have been left unmasked in Figures 12. The aurora is seen in emissions of $N_2^+$ at 391.4 nm in the UV band (Figure 12a) and O at 557.7 nm in the VIS band (Figure 12b). A prominent nightglow layer is seen just below 100 km altitude and auroral light is seen up to about 160 km above the surface, consistent with ground-based observations of the altitude of O(557.7 nm) emissions at similar latitudes (Whiter et. al., 2022). Evidence of other expected lines (Chamberlain, 1961; Jones, 1971) also appears in spatially averaged spectra at lower significance. Expected O(630.0 nm) lines and the Na D lines are indicated in Figure 12d. Light from the doublet Na D lines (589.0 nm and 589.6 nm, within the ~0.6-nm spectral resolution of TEMPO) appears to be found in the lower (nightglow) layer near where it is expected. The UV band is expected to include lines from $N_2^+$ at 391.4 nm and 427.8 nm, as well as other lines. Our spatially averaged spectra show these lines and are in good agreement with data from the limb-viewing OSIRIS spectrometer on Odin (Wild, 2006) and ground observations (Yoshinuma et. al., 2024). There is strong evidence for a 391.4-nm line in our data, which is in the spectral range where the TEMPO background signal is relatively smaller (Figure 8). The larger background at the 427.8 nm wavelength reduces the significance of the longer wavelength $N_2^+$ line due to residual unsubtracted background and excess Poisson noise from the subtracted background. The TEMPO data also becomes noisy at wavelengths > 640 nm.

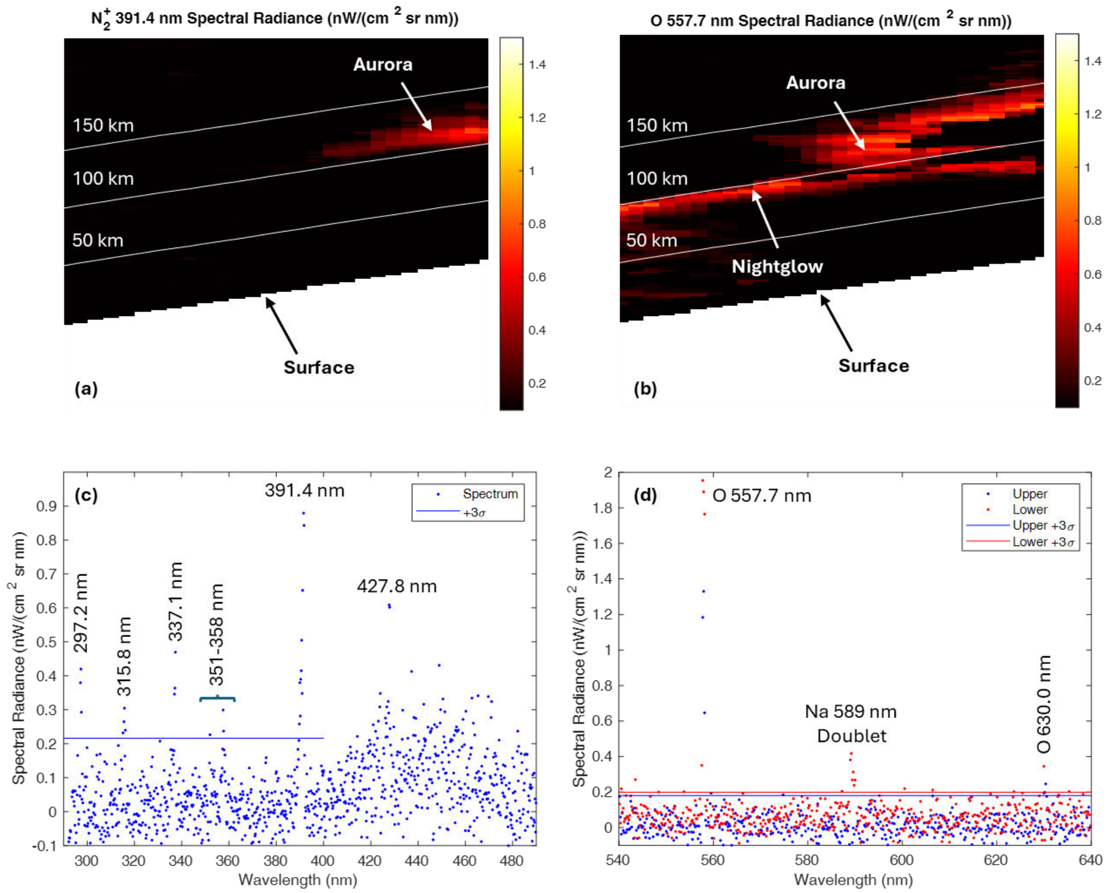


**Figure 12**. Nightglow and auroral imagery for 11 March 2024 10:33Z extends to the limb at (65.6°N, 153.8°W) and beyond into space. Panel (a) shows $N_2^+$(391.4 nm) light and panel (b) shows (O557.7 nm) light. Panels (c) and (d) are spatially averaged spectra. Panel (c) averages over the auroral region while panel (d) separates the nightglow (lower) and auroral (upper) regions. The spectral radiances in panels (a) and (b) sum the five spectral bins centered around the indicated lines.

### 4.4 Gas Flaring

Gas flaring associated with oil and gas production can be seen several places in TEMPO nighttime datasets. Figure 13 is an example from an offshore platform. The signature of flaring is an approximate blackbody spectrum of a hot source, in this case, one at 1600 K, which is expected (Elvidge et. al., 2013). Atmospheric absorption features reduce the observed radiance above 680 nm. Other hot sources, such as refining operations and wildfires should be similarly observable.

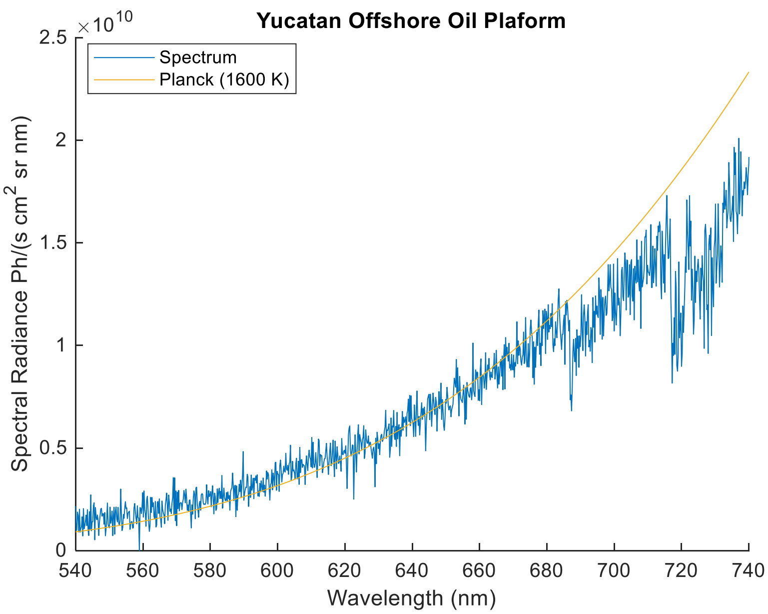


**Figure 13.** Flaring off the coast of the Yucatan with a blackbody spectrum that approximates the observed spectrum below 680 nm. Atmospheric absorption affects the spectrum above 680 nm. Observation is at 2024 March 15 01:42:08Z, Scan 17, Granule 5, Step 103, Pixel 1896.

4.6 Lightning

Lightning is considered an essential climate variable (ECV) by the World Meteorological Organization's Global Climate Observing System **(**GCOS**)**. The World Wide Lightning Location Network (WWLN) and Earth Networks Total Lightning Network **(**ENTLN**)** are examples of ground-based global lightning detection using impulsive very-low-frequency (VLF) radiation discharges from lightning called sferics. Satellite-based lightning detection (e.g., Albrecht et al., 2016) utilize optical (light) signals, and particularly a characteristic near-infrared emission signal at 777.4 nm. Notable satellite-based lightning-detection sensors including the Optical Transient Detector (OTD; Christian et al., 1996) on NASA's MicroLab-1 satellite, the Lightning Imaging Sensor (LIS) on the Tropical Rainfall Measuring Mission (TRMM; Kummerow et al., 1998), and the Geostationary Lightning Mapper (GLM; Goodman et al., 2013) on the Geostationary Operational Environmental Satellite (GOES) R-Series. Given that TEMPO is sufficiently sensitive to capture both city lights and lunar reflection from clouds, it is expected that lightning would be detectable too.

Apart from the 777.4 nm emission line, which is detectable day and night by the aforementioned sensors designed to measure lightning, low-light-sensitive broadband (e.g., 500-900 nm) visible sensors such as the Operational Linescan System (Orville and Henderson, 1986) and the VIIRS-DNB (Miller et al., 2013) demonstrate a limited ability to capture lightning flashes as well. Unlike the charge-coupled device (CCD) detector arrays employed by the OTD, LIS, and GLM, which offer an ability to "stare" at the scene and provide a two-dimensional view of lightning flash morphology, the OLS and VIIRS-DNB are cross-track scanning radiometers and can detect only a fortuitous portion of the transient diffused-light from lightning flashes as they scan rapidly across the cloud top. Thus, these scanning sensors detect only a subset of the total flash activity. These flashes appear in OLS and DNB nighttime imagery as a series of along-scan pixels (relatively bright “line segments”; see Figure 13 of Miller et al., 2013). These scanning sensors are mentioned here because the way TEMPO detects lightning can be thought of as a hybrid between the CCD and scanning approaches, yielding its own unique way of observing a flash.

Figure 14 shows a comparison between GLM, TEMPO, and VIIRS-DNB lightning detections for a temporally matched nighttime scene on 15 October 2024 over the eastern coast of the continental U.S. and a portion of the northwestern Atlantic Ocean. Figure 14a shows a GOES-16 Advanced Baseline Imager GeoColor (Miller et al., 2020) image with GLM Group Energy Density overlaid, showing a line of storms over the Gulf Stream area of the Atlantic that produced frequent lightning flashes around 01:10Z. In the TEMPO imagery (Figure 14b), lunar reflection shows the same line of convective cloud tops, and within these clouds there appears a series of vertically oriented bright linear segments. These segments correspond closely to the GLM-identified lightning flashes. Figure 14c with inset 14d shows how the DNB observed this same convective line when NOAA-20 crossed over the northwestern Atlantic region several hours later (~06:20Z). Recall that in DNB imagery, lightning flashes appear as along-scan bright segments. Assuming that the average flash rate of the convective line is similar between the time of the GLM/TEMPO and DNB imagery (deemed reasonable based on GLM observations available at both 01:10Z and 06:20Z), it is noteworthy that TEMPO detected much more lightning activity (roughly 10 times more, in this case) than the 1-2 flashes detected by the DNB. The increased detection rate is presumably due to the much longer exposure (dwell) time (~6s) of TEMPO compared to the ~25-50 ms time for the DNB to traverse a 10-20 km cloud top (based on ~2.68 ms/pixel dwell time; Elvidge et al., 2022). Thus, TEMPO is a more efficient detector of lightning than the DNB, albeit a much less efficient detector than a sensor designed for that purpose (GLM).

GLM collects images every 2 ms and is therefore designed to capture at least 70% of lightning flashes within its field of view. Similar to the OLS/DNB example, the step-and-stare design of TEMPO, which employs a tall (North/South) CCD and a narrow (East/West) slit, allows only a small subset of the total lightning to be detected; specifically, whatever flashes happen to occur within the ~4.75 km wide view of the slit during the exposure at each step. Unlike the OLS and DNB, in TEMPO’s scanning strategy the flashes appear as ~North/South oriented segments, since a flash will illuminate a relatively large area atop a convective cloud top. City lights seen by TEMPO along the eastern coast of the U.S. can compared with the GeoColor imagery (which employs a static city light database) to help with geolocation in this example, since the two images are not co-registered.

Lightning spectra are known to contain many atomic and molecular lines that TEMPO can observe (Salanave, 1961; Wallace, 1960; Walker and Christian, 2014; Kieu et.al., 2021). The line at 777.4 nm used by GLM is unfortunately outside TEMPO’s spectral range. Lightning spectral features are particularly prominent on the UV side as is shown in Figure 15 even with moonlight illuminating the cloud tops.

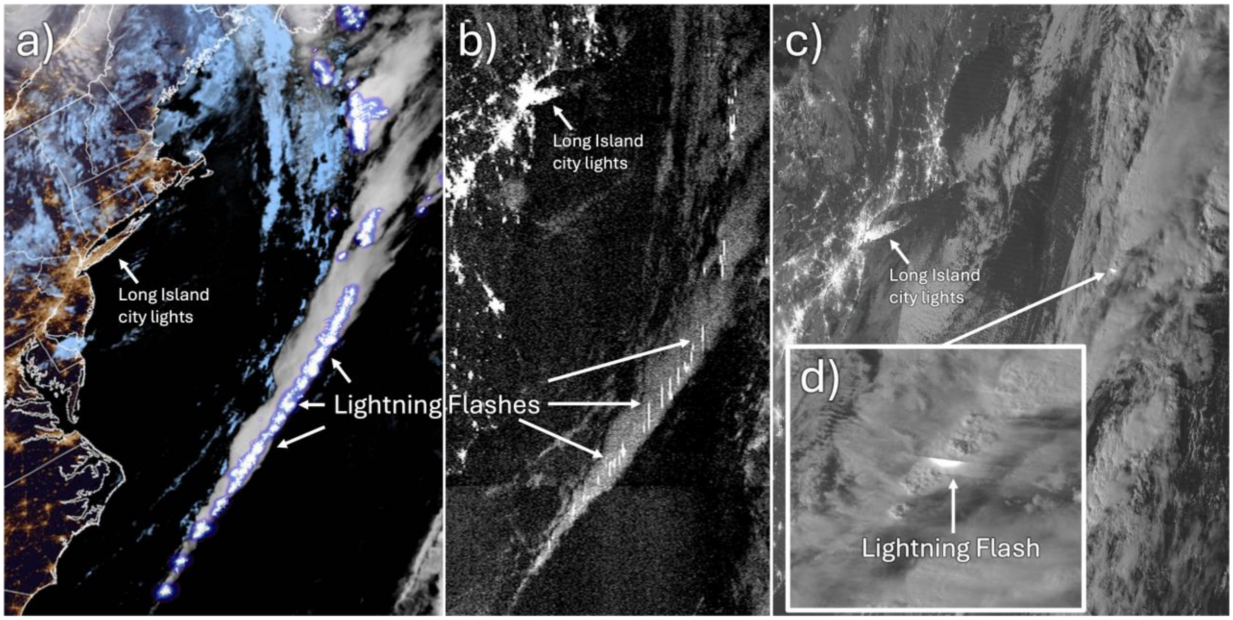


**Figure 14**. Panel (a) shows the GOES-16 Advanced Baseline Imager GeoColor image from 15 October 2024 01:10Z with Geostationary Lightning Mapper Group Energy Density overlaid, and panel (b) shows a TEMPO image from 15 October 2024 01:04Z using 6 second exposures. Panel (c) with inset (d) shows NOAA-20 VIIRS-DNB imagery from 15 October 2024 at 06:20Z. Note: imagery are on different map projections but display roughly the same domain (using city lights as landmarks).

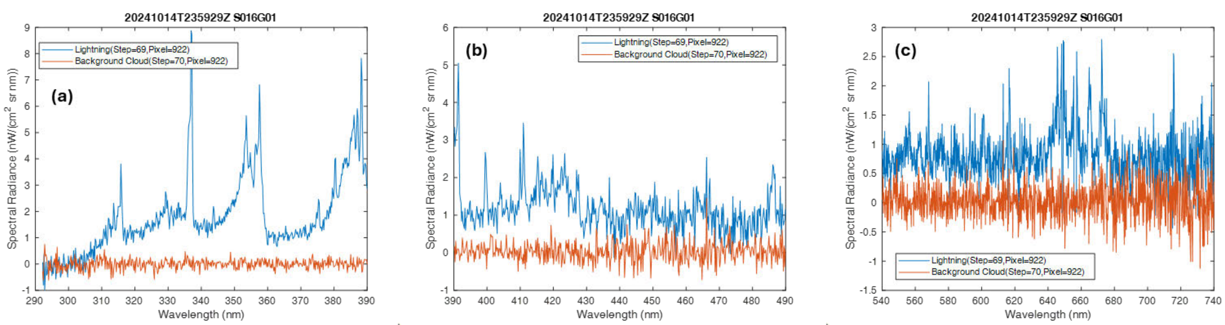


**Figure 15**. Lightning pixel spectrum shown (blue) with the spectrum of a neighboring pixel (red) sampled 6 s after lightning illuminated the cloud top as background for comparison. Panel (a) shows the UV spectrum, (b) shows UV-blue, and (c) shows the VIS side of the spectrum.

## 5 Conclusions

TEMPO is proving to be a capable instrument for studying the Earth at night in the UV and visible wavelengths. As we have demonstrated, it can make observations of city lights, nightglow and aurorae, moonlit clouds, gas flares, and lightning and provide a rich set of spectral information from which spectral classifications can be made, combustion temperatures can be estimated, and processes relating to nightglow, aurorae, and lightning strokes can be studied. It is the hope of the authors that many will find these topics interesting and begin to use TEMPO at night, which is an opportunity that was never envisioned at the time TEMPO was proposed as an Earth Venture Instrument for atmospheric chemistry and air quality.

TEMPO nighttime data are available as twilight radiances from ASDC. Postprocessing of the Version 3 twilight radiances is needed to extract the nighttime signals, including masking permanently and transiently hot pixels, and background subtraction to remove residual dark current (including variations with CCD temperature) and scattered light from the bright side of the terminator that enters as stray light. The algorithms for the postprocessing have been described in Section 2.4 and the Python code implementing it is available on GitHub.

## Acknowledgments

TEMPO is supported by NASA Earth System Science Pathfinder (ESSP) Earth Venture Instrument Program, under the Earth Science Division of the Science Mission Directorate (Contract No. NNL13AA09C). We would like to acknowledge the contributions of the entire TEMPO team including TEMPO instrument project, TEMPO mission project, BAE Systems, Inc. Space & Mission Systems (formerly Ball Aerospace), and partners MAXAR Technologies and Intelsat for enabling the TEMPO mission, and NASA's Atmospheric Science Data Center (ASDC) for the archival and distribution of TEMPO data products including twilight radiances. SAO authors would like to thank the NASA Satellite Needs Working Group for some support under the TEMPO Near-Real-Time (NRT) Project (Contract No. 80MSFC24CA004**)**.

JLC and HM would like to thank the NASA Earth Science Technology Office for supporting some of this work under the Advanced Information Systems Technology (AIST) program (now Intelligent Systems Technology), Grant No. 80NSSC22K1156, Dr. Jacqueline Le Moigne, program officer.

DLW would like to acknowledge NASA's support for the development of the Pandora instrumentation and Sun-Climate research.

We acknowledge the use of imagery from the NASA Worldview application (https://worldview.earthdata.nasa.gov), part of the NASA Earth Science Data and Information System (ESDIS).

The views, opinions, and findings contained in this report are those of the authors and should not be construed as an official National Oceanic and Atmospheric Administration or United States Government position, policy, or decision.

The authors have no conflicts of interest to declare.

## Open Research

All data used in this article is publicly available from the NASA Atmospheric Science Data Center (ASDC) https://asdc.larc.nasa.gov/project/TEMPO. Postprocessing code needed to mask hot pixels and subtract the background signal to produce clean TEMPO nighttime radiances is found in GitHub https://github.com/Smithsonian/TEMPO-Twilight-processing/tree/main.

## References


Albrecht, R. I., S. J. Goodman, D. E. Buechler, R. J. Blakeslee, and H. J. Christian (2016). Where Are the Lightning Hotspots on Earth? *Bull. Amer. Meteor. Soc*., 97, 2051–2068, https://doi.org/10.1175/BAMS-D-14-00193.1

ASDC https://asdc.larc.nasa.gov/project/TEMPO

BlackMarble https://blackmarble.gsfc.nasa.gov/

Carr, J., Liu, X., Baker, B. and Chance, K. (2017). Observing nightlights from space with TEMPO. International Journal of Sustainable Lighting, 19(1), pp.26-35. https://doi.org/10.26607/ijsl.v19i1.64

Chance, K., Liu, X., Miller, C.C., Abad, G.G., Huang, G., Nowlan, C., Souri, A., Suleiman, R., Sun, K., Wang, H., Zhu, L., et al. (2019). TEMPO Green Paper: Chemistry, physics, and meteorology experiments with the Tropospheric Emissions: monitoring of pollution instrument. In *Sensors, systems, and next-generation satellites XXIII* (Vol. 11151, pp. 56-67). SPIE. https://doi.org/10.1117/12.2534883

Chakraborty, S., Oda, T., Kalb, V.L., Wang, Z., & Román, M.O. (2023). Potentially underestimated gas flaring activities—a new approach to detect combustion using machine learning and NASA's Black Marble product suite. Environmental Research Letters 18, 3, 035001. https://doi.org/10.1088/1748-9326/acb6a7

Chamberlain, J.W., 2016. *Physics of the Aurora and Airglow: International Geophysics Series, Vol. 2* (Vol. 2). Elsevier.

Christian, H. J., K. T. Driscoll, S. J. Goodman, R. J. Blakeslee, D. A. Mach, and D. E. Buechler (1996). The Optical Transient Detector (OTD), *Proceedings of the 10th International Conference on Atmospheric Electricity*; Osaka, Japan; June 10-14, 1996; pp 368-371.

Ditmer, M.A., Stoner, D.C., & Carter, N.H. (2021, May). Estimating the loss and fragmentation of dark environments in mammal ranges from light pollution. Biological Conservation, 257, 109135. https://doi.org/10.1016/j.biocon.2021.109135

Elvidge, C.D., Keith, D.M., Tuttle, B.T. and Baugh, K.E. (2010). Spectral identification of lighting type and character. *Sensors*, *10*(4), pp.3961-3988. https://doi.org/10.3390/s100403961

Elvidge, C.D., Zhizhin, M., Hsu, F.C. and Baugh, K.E. (2013). VIIRS nightfire: Satellite pyrometry at night. *Remote Sensing*, *5*(9), pp.4423-4449. https://doi.org/10.3390/rs5094423

Elvidge, C. D., M. Zhizhin, D. Keith, S. D. Miller, F. C. Hsu, T. Ghosh, S. Anderson, C. K. Monrad, M. Bazilian, J. Taneja, P. C. Sutton, J. Barentine, W. S. Kowalik, C. C. M. Kyba, D. W. Pack, and D. Hammerling (2022). The VIIRS Day/Night Band: A Flicker Meter in Space? *Remote Sensing*, 14(6) 1316. https://doi.org/10.3390/rs14061316

ENTLN https://www.earthnetworks.com/why-us/networks/lightning/

GitHub https://github.com/Smithsonian/TEMPO-Twilight-processing/tree/main

Goodman, S. J., R. J. Blakeslee, W. J. Koshak, D. Mach, J. Bailey, D. Buechler, L. Carey, C. Schultz, M. Bateman, E. M., Jr., and G. Stano (2013) The GOES-R Geostationary Lightning Mapper (GLM). *Atm. Research*, 125-126, 34-49. https://doi.org/10.1016/j.atmosres.2013.01.006

GCOS https://gcos.wmo.int/en/essential-climate-variables/lightning

Huber, P.J. and Ronchetti, E.M. (2011). *Robust statistics*. John Wiley & Sons.

Jones, A.V. (1971). *Auroral Spectroscopy*. Space Science Reviews, *11*(6), pp. 776-826. https://doi.org/10.1007/BF00216890

Kieu, N., Gordillo-Vázquez, F.J., Passas, M., Sánchez, J. and Pérez-Invernón, F.J., 2021. High-speed spectroscopy of lightning-like discharges: Evidence of molecular optical emissions. *Journal of Geophysical Research: Atmospheres*, *126*(11), p.e2021JD035016. https://doi.org/10.1029/2021JD035016

Kummerow, C., W. Barnes, T. Kozu, J. Shiue, and J. Simpson, 1998: The Tropical Rainfall Measuring Mission (TRMM) Sensor Package. J. Atmos. Oceanic Technol., 15, 809–817, https://doi.org/10.1175/1520-0426(1998)015<0809:TTRMMT>2.0.CO;2

Levin, N., Kyba, C.C., Zhang, Q., de Miguel, A.S., Román, M.O., Li, X., Portnov, B.A., Molthan, A.L., Jechow, A., Miller, S.D. and Wang, Z., 2020. Remote sensing of night lights: A review and an outlook for the future. *Remote Sensing of Environment*, *237*, p.111443. https://doi.org/10.1016/j.rse.2019.111443

Lin, G., Wolfe, R.E., Zhang, P., Dellomo, J.J. and Tan, B., 2022. Ten years of VIIRS on-orbit geolocation calibration and performance. *Remote Sensing*, *14*(17), p.4212. https://doi.org/10.3390/rs14174212

Martinez, J. F., MacManus, K., Stokes, E., Wang, Z., & de Sherbinin, A. (2023). Suitability of NASA's Black Marble Daily Nighttime Lights for Population Studies at Varying Spatial and Temporal Scales. Remote Sensing, 15(10), 2611. https://doi.org/10.3390/rs15102611

Miller, S. D., W. S., III, S. P. Mills, C. D. Elvidge, T. F. Lee, J. Solbrig, A. Walther, A. K. Heidinger, and S. C. Weiss, 2013: Illuminating the Capabilities of the Suomi National Polar-Orbiting Partnership (NPP) Visible Infrared Imaging Radiometer Suite (VIIRS) Day/Night Band. *Remote Sens.*, 5(12), 6717-6766. https://doi.org/10.3390/rs5126717

Miller, S. D., D. T. Lindsey, C. J. Seaman, and J. E. Solbrig, 2020: GeoColor: A Blending Technique for Satellite Imagery. J. Atmos. Ocean. Tech., 37(3), 429-448, https://doi.org/10.1175/JTECH-D-19-0134.1

Orville, R. E., and R. W. Henderson, 1986: Global distribution of midnight lightning: September 1977 to August 1978. Mon. Wea. Rev.,114, 2640–2653. https://doi.org/10.1175/1520-0493(1986)114%3C2640:GDOMLS%3E2.0.CO;2

PGN https://www.pandonia-global-network.org

Rogers, M.A., Miller, S.D., Seaman, C.J., Torres, J., Hillger, D., Szoke, E. and Line, W.E., 2023. VIIRS after 10 Years—A Perspective on Benefits to Forecasters and End-Users. *Remote Sensing*, *15*(4), p.976. https://doi.org/10.3390/rs15040976

Ryan, R.E., Pagnutti, M., Ryan, H., Burch, K. and Manriquez, K., 2024. Satellite Hyperspectral Nighttime Light Observation and Identification with DESIS. *Remote Sensing*, *16*(5), p.923. https://doi.org/10.3390/rs16050923

Salanave, L.E., 1961. The Optical Spectrum of Lightning: A revival of the spectrographic study of lightning may help solve some outstanding puzzles in could physics. *Science*, *134*(3488), pp.1395-1399. https://doi.org/10.1126/science.134.3488.1395

Smith, D.R., Holland, A.D. and Hutchinson, I.B., 2004. Random telegraph signals in charge coupled devices. *Nuclear Instruments and Methods in Physics Research Section A: Accelerators, Spectrometers, Detectors and Associated Equipment*, *530*(3), pp.521-535. https://doi.org/10.1016/j.nima.2004.03.210

Tapia Ayuga, C., Sánchez de Miguel, A. and Zamorano Calvo, J., 2017. *LICA-UCM lamps spectral database*. Grupo UCM de Astrofísica Extragaláctica e Instrumentación Astronómica. https://hdl.handle.net/20.500.14352/22872

VIIRS-DNB https://www.earthdata.nasa.gov/learn/backgrounders/nighttime-lights

Walker, T.D. and Christian, H.J., 2014, June. Novel observations in lightning spectroscopy. In *XV International Conference on Atmospheric Electricity, Norman, Oklahoma*. https://www.nssl.noaa.gov/users/mansell/icae2014/preprints/Walker_292.pdf

Wallace, L., 1960. Note on the spectrum of lightning in the region 3670 to 4280 A. *Journal of Geophysical Research*, *65*(4), pp.1211-1214. https://doi.org/10.1029/JZ065i004p01211

Wang, Z., Román, M.O., Sun, Q., Molthan, A.L., Schultz, L.A., and Kalb, V.L. (2018). Monitoring Disaster-Related Power Outages Using NASA Black Marble Nighttime Light Product, Int. Arch. Photogramm. Remote Sens. Spatial Inf. Sci., XLII-3, 1853–1856. https://doi.org/10.5194/isprs-archives-XLII-3-1853-2018

Whiter, D. K., Partamies, N., Gustavsson, B., and Kauristie, K.: The altitude of green OI 557.7 nm and blue $N_2^+$ 427.8 nm aurora, Ann. Geophys., 41, 1–12, https://doi.org/10.5194/angeo-41-1-2023

Wild, J., 2006. Look out, aurorae about!. *Astronomy & Geophysics, Volume 47, Issue 1, pp. 1.11-1.13.*, *47*(1), pp.1-11. https://doi.org/10.1111/j.1468-4004.2006.47111.x

WWLN https://wwlln.net/

Yoshinuma, M., Ida, K. and Ebihara, Y., 2024. Development of hyperspectral camera for auroral imaging (HySCAI). *Earth, Planets and Space*, *76*(1), p.96. https://doi.org/10.1186/s40623-024-02039-y

Yu, Y., Liu, S., Li, Y., & Shi, K. (2023). Satellite Remotely Sensed Nighttime Lights Reveal Spatiotemporal Dynamics of the Ukrainian-Russian Conflict. IEEE Geoscience and Remote Sensing Letters, 20, 1-5. https://doi.org/10.1109/LGRS.2023.3290559

Zhang, D., Huang, H., Roy, N, Roozbahani, M.M., Frost, J.D. (2023). Black Marble Nighttime Light Data for Disaster Damage Assessment. Remote Sensing. 15(17), 4257. https://doi.org/10.3390/rs15174257

Zhou, M., Wang, J., Chen, X., Xu, X., Colarco, P.R., Miller, S.D., Reid, J.S., Kondragunta, S., Giles, D.M. and Holben, B., 2021. Nighttime smoke aerosol optical depth over US rural areas: First retrieval from VIIRS moonlight observations. *Remote Sensing of Environment*, *267*, p.112717. https://doi.org/10.1016/j.rse.2021.112717

Zoogman, P., Liu, X., Suleiman, R.M., Pennington, W.F., Flittner, D.E., Al-Saadi, J.A., Hilton, B.B., Nicks, D.K., Newchurch, M.J., Carr, J.L. Janz, S.J., et al., 2017. Tropospheric emissions: Monitoring of pollution (TEMPO). Journal of Quantitative Spectroscopy and Radiative Transfer, 186, pp.17-39. https://doi.org/10.1016/j.jqsrt.2016.05.008